Microstructure of directionally solidified high-critical-current $YBa_2Cu_3O_7$-Y_2BaCuO_5 composites

Felip Sandiumenge
Institut de Ciencia de Materials de Barcelona, Consell Superior d'Investigacions Científiques, Campus de la Universitat Autònoma de Barcelona, 08193 Bellaterra, Catalunya, Spain and Centre d'Elaboration de Materiaux et d'Etudes Structurales, Centre National de la Recherche Scientifique, 29, rue Jeanne Marvig, 31055 Toulouse, Cedex, France

Salvador Piñol and Xavier Obradors
Institut de Ciencia de Materials de Barcelona, Consell Superior d'Investigacions Científiques, Campus de la Universitat Autònoma de Barcelona, 08193 Bellaterra, Catalunya, Spain

Etienne Snoeck and Christian Roucau
Centre d'Elaboration de Matériaux et d'Etudes Structurales, 29, rue Jeanne Marvig, 31055 Toulouse, Cedex, France
(Received 2 March 1994)

The complex microstructure of directionally solidified $YBa_2Cu_3O_7$-Y_2BaCuO_5 composites having up to 30 vol % 2:1:1 precipitates with sizes down to 0.1 μm and critical currents above 10^5 A/cm^2 at 77 K and zero magnetic field has been investigated through detailed transmission electron microscopy observations. It is shown that samples with a high Y_2BaCuO_5 concentration display polygonization as a mechanism to relieve stress while only small microcracks occur which are very efficiently stopped by small Y_2BaCuO_5 precipitates. This crystal polygonization leads to the formation of either sharp or diffuse interfaces within the $YBa_2Cu_3O_7$ matrix. In the first case low angle grain boundaries occur which have a minor perturbation of the critical currents, while strongly disordered smooth interfaces are observed in other cases which because of their irregular distribution can only have a minor relevance on the flux-pinning mechanism of these superconductors. Stacking faults are found to be a common defect in the $YBa_2Cu_3O_7$ matrix but they are very inhomogeneously distributed thus preventing to establish a clear correlation between their density and critical currents. The formation mechanism of these stacking faults is discussed on the basis of their observed distribution. Sharp $Y_2BaCuO_5/YBa_2Cu_3O_7$ interfaces have been observed at the atomic level, even if a high density of stacking faults and dislocations occur at certain orientations of the interfaces. Owing to the homogeneous distribution of these sharp interfaces we conclude that they constitute the dominant pinning mechanism at low magnetic fields in the $YBa_2Cu_3O_7$-Y_2BaCuO_5 composites.

I. INTRODUCTION

The attainment of high-critical-current densities in high-temperature superconductors is a long standing issue of current interest. Melt-texture processing of $YBa_2Cu_3O_7$ (1:2:3) is now one of the more promising techniques with which to overcome the limitations associated with grain-boundary weak-link behavior and to increase the macroscopic pinning force through the introduction of artificial pinning centers such as Y_2BaCuO_5 (2:1:1). It is well known that the physical properties of melt-processed 1:2:3-2:1:1 composites are especially sensitive to their microstructure. The resulting microstructural features, in turn, are established through the different steps of the sample preparation process. Sample solidification, cooling, and subsequent annealing, induce the development of specific defects which interact along with the thermal evolution of the sample; therefore an understanding of each process separately may allow a better control of the sample's microstructure and therefore its properties. Several studies have been reported on the possible influence of discrete defects on the resulting critical-current density J_c. However, to date little is known about the microstructural evolution of the sample from its solidification up to its final form in directionally solidified samples. By way of introduction first we briefly summarize the present knowledge on the microstructure and its implications on J_c of melt-textured 1:2:3-2:1:1 composites, and secondly define the detailed microstructural investigation of high-critical-current directionally solidified composites presented in this article.

A. Previous investigations

The fabrication of aligned 1:2:3-2:1:1 composites with relatively few weakly linked boundaries has already been accomplished by several groups,[1-14] using techniques which include slow cooling of a static sample through the 2:1:1 + liquid $\rightarrow$ 1:2:3 peritectic temperature (melt-texture growth,[1,2] melt-powder-melt-growth (MPMG),[3,4] directional solidification of extruded rods,[5] Bridgman solidification,[6-8] zone melting,[9-12] and melt texturing of thick films on Ag 10% Pd alloy substrates.[13,14] Early studies of the microstructure of melt-processed samples have indicated that single domains consist of many

stacked platelets having a common c axis, defining a "brick-wall" microstructure;[15] rotations around this common or nearly common c axis result in twist boundaries between stacked platelets.[15] However, the brick-wall description has been abandoned after the work by Alexander *et al.*,[16] who demonstrated that single domains consist of interconnected single-crystalline material. Further confidence for this idea came from the observation that transport current flow along the c axis direction was not weak-link limited.[17] It appeared that gaps between adjacent platelets terminate within domains and contain entrapped solidified melt.[16] Transmission electron microscopy (TEM) and polarized optical microscopy observations of as-solidified material and quenched solid-liquid interfaces supported a growth model which accounts for such a platelet microstructure.[16,18,19] In brief: The anisotropic growth rate parallel and perpendicular to the c axis leads to the formation of parallel platelets thin along the c axis separated by gaps; interaction between advancing platelets and 2:1:1 particles make the gaps to preferentially terminate at 2:1:1/1:2:3 interfaces. Following this solidification scenario, the generation of low angle grain boundaries within single domains of melt-processed 1:2:3-2:1:1 composites is expected to result from slight misorientations between individually solidified adjacent platelets. We have shown recently, that this growth mechanism ceases to be operative for specific cases where the growth front is highly constrained in space and for relatively large concentrations of 2:1:1 particles in the melt,[20] leading to distinctive microstructural features to be discussed in this paper.

Many efforts have been directed towards an estimation of the effect on J_c of individual defects, namely, twin planes,[21,22] dislocations,[23,24] stacking faults,[25,26] oxygen deficiencies,[27] and 2:1:1 precipitates.[28] Magnetization measurements performed on single domains of MPMG samples indicated that J_c at 77 K scales with the effective 2:1:1/1:2:3 interface area.[28] The idea that 2:1:1 precipitates can act themselves as pinning centers, however, seems not to be realistic after considering that their size is about 2 orders of magnitude larger than the coherence length in 1:2:3.[29–31] Alternatively, it may be argued that it is the 2:1:1/1:2:3 interface, where the free-energy gradient is a maximum, which acts as pinning center.[28,32] This mechanism predicts an increase of J_c with increasing the total effective 2:1:1/1:2:3 interface area. Such a behavior has been indeed found in our samples.[33]

The main controversy at this point is whether the 2:1:1/1:2:3 interface itself or defects associated with it act as effective vortex pinning centers. From TEM observations[34] and Fourier transforms of crystal-lattice images[35] of the 1:2:3 matrix around 2:1:1 precipitates, it was concluded that neither strain nor lattice defects are generated in the matrix adjacent to precipitates. However, defects around 2:1:1 precipitates can arise either from the elastic and thermal-expansion anisotropy between the trapped precipitates and the matrix,[36] and the inherent thermodynamical driving force for the dissolution of the metastable 2:1:1 precipitates.[26] In particular, TEM observations have revealed that the density of dislocations may be increased locally around 2:1:1 precipitates.[37,38] The pinning mechanism by dislocations was recently considered in detail.[24,39] Moreover, TEM and energy dispersion spectroscopy (EDS) experiments performed on melt-textured thick films deposited on Ag 10% Pd substrates showed a pronounced increase of the density of stacking faults close to 2:1:1/1:2:3 interfaces as well as a yttrium-enriched thin layer adjacent to 2:1:1 boundaries which could be a vestige of a high concentration of point defects around 2:1:1 precipitates.[26] Such increased stacking-fault density around 2:1:1 precipitates was suggested to contribute significantly to the bulk pinning efficiency of the sample, thus providing a possible alternative explanation to the correlation between 2:1:1/1:2:3 interface area and J_c.

B. Questions addressed by current work

Previous observations of quenched as-grown directionally solidified samples[20] revealed a growth mode distinct from that postulated by Goyal *et al.*[18] Therefore the first issue to be discussed below concerns the observation of distinctive microstructural features characteristic of our directionally solidified samples. As-solidified tetragonal samples do not display the platelet microstructure, but under the polarized light microscope and TEM they appear as homogeneous single-crystalline material along the three crystallographic directions. For a sufficiently large 2:1:1/1:2:3 interface area, the stress associated with the anisotropic thermal contraction is relieved by polygonization.[23,40] With this information, one can better interpret the physical properties measured on samples processed under different conditions and controllably manipulate solidification and subsequent thermal cycling to achieve desired properties.

As mentioned above, stacking faults have been proposed to contribute to flux pinning.[25,26] We will justify that stacking faults can be formed at different stages of the sample preparation process, first as Cu excess in the 1:2:3 material incorporated during solidification, and second as decomposition byproduct of 2:1:1 precipitates during subsequent annealing. Both generation processes are difficult to control and apparently there is no means to determine which process limits the resulting stacking-fault density.

Next, the 2:1:1/1:2:3 interface is considered in detail and the results are justified within the theoretical framework developed for the incorporation process of solid particles into an advancing solid-liquid interface.[41] Our results allow us to attempt a cronology of events which lead to the final microstructural features of the 2:1:1/1:2:3 interface. Finally, implications of the details of the observed microstructure on the measured critical current density J_c will be discussed.

II. EXPERIMENTAL

Presintered 1:2:3 and 2:1:1 precursors were thoroughly mixed, shaped to a semicylinder of 12 cm in length and 0.3 cm in diameter and sintered in a constant temperature furnance. The initial composition of the ceramic composite was varied from 0 to 40% in weight of the

2:1:1 phase. The ceramic bar was suspended in a tubular furnance working in air with a vertical Bridgman configuration. The furnace was heated to a maximum temperature typically 1150 °C and the sintered bars were displaced at a constant rate of $R = 1$ mm/h in a region having an axial temperature gradient of $G = 20$ °C/cm until the full length of the bar was cooled down to a temperature of 900 °C. These conditions correspond to an optimized $G/R = 0.07 \times 10^7$ K s/cm^2 ratio. A brief description of the sample preparation procedure is reported elsewhere.[8] It is important to stress that within our experimental resolution we did not detect any lateral temperature gradient in the furnance within the space reserved to the sample. In our experimental setup, the partially melted bar is suspended vertically and held by capillary forces. Therefore, the maximum working temperature during the experiment is determined by the maximum temperature for which the partially melted ceramic bar can be suspended without losing its mechanical stability.

The top of the solidified bars usually displayed a polynucleation zone with a length, which depends on the 2:1:1 concentration, of about 2–3 cm where growth competition between domains takes place. Below this region, typically a single domain of about 9 cm in length was obtained. Figure 1 shows a typical bicrystal with ~15 vol % 2:1:1 corresponding to two different growth fronts having the *a-b* planes (parallel to the microcracks) inclined about 45° to the vertical axis of the furnace. Even the resulting single-domain region typically displayed such a deviation.

The final content of the 2:1:1 phase in the ceramic composite was determined by measuring the paramagnetic susceptibility of the composite and fitting a Curie-Weiss law in the high-temperature range ($T > 120$ K).

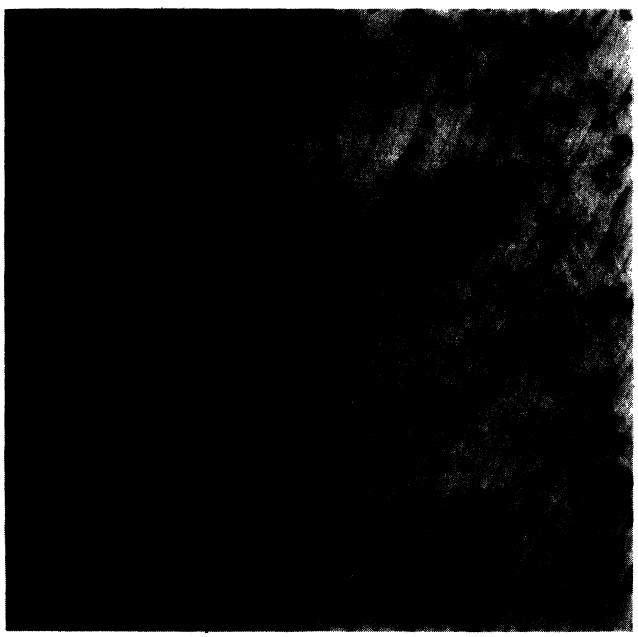

FIG. 1. Grain boundary corresponding to two domains misoriented by 90° in a sample with ~15 vol % 2:1:1. The growth axis is vertical. Scale bar represents 50 μm.

Then the actual 2:1:1 phase percentage may be obtained through the relation $(\mu_{\text{observed}}/\mu_{2:1:1})^2 \times 100$, μ_{observed} being the magnetic moment obtained from the Curie-Weiss law and $\mu_{2:1:1}$ the magnetic moment of the 2:1:1 pure phase. In this paper we mainly study samples with ~30 vol % 2:1:1 and in specific cases indicated in the text, we also use samples with 15 vol % 2:1:1 in order to compare their microstructure.

Inductive critical currents were measured with a superconducting quantum interference device magnetometer in several samples having different concentration and size of 2:1:1 precipitates. J_c values up to 10^5 A/cm^2 at 77 K and 2×10^6 A/cm^2 at 5 K were found, both at zero magnetic field, thus indicating an enhanced pinning behavior.[8,33]

Observations of the microstructure were performed using a polarized light optical microscope on polished samples, and using TEM. Samples for TEM where cut from the textured bars with a diamond saw. Care was taken to avoid contact of the specimens with water at all times. The slices were mechanically polished down to ~30 μm and ion milled at reduced voltages (5 kV) and currents (0.3 mA) and cooled by a cold finger immersed in liquid nitrogen to avoid damage of the samples. We have indeed verified that the observed microcracks are intrinsic defects in our orthorhombic 1:2:3 samples with about 30 vol % 2:1:1 and not artifacts introduced during the ion-milling process; this is for instance evidenced by the fact that such microcracks were not observed during an investigation of tetragonal 1:2:3 samples without 2:1:1 addition thinned by the same procedure. TEM observations and selected area diffraction (SAD) were performed on the Philips CM20 and CM30 electron microscopes at 200 and 300 kV, respectively. Chemical compositions of the different phases were deduced from EDS. Finally, in order to detect any possible preferential orientation or texture of the 2:1:1 precipitates embedded in the 1:2:3 matrix, the room-temperature electron-spin-resonance (ESR) spectra of a sample composite having ~30 vol % 2:1:1 was measured with the external field applied perpendicular and parallel to the *c* axis of the 1:2:3 matrix.

III. RESULTS AND DISCUSSION

A. Matrix defects

The microstructure of the matrix is highly dependent on the concentration and size of 2:1:1 precipitates. Figure 1 shows a polarized light micrograph of a sample containing ~15 vol % 2:1:1. The samples contain precipitates with diameters typically between 5 and 15 μm, and large scale microcracks (the term large scale microcracks is used hereafter to indicate microcracks which are visible under the optical microscope at a magnification of ×1000). In contrast, large scale microcracks are completely suppressed when the concentration of the 2:1:1 phase is raised up to ~30 vol %, as illustrated in Fig. 2 for a sample grown under identical conditions as that shown in Fig. 1. Instead, small microcracks are formed (not observable under the optical microscope, see below) which are densely distributed through the sample. The average spacing along the *c* axis between these mi-

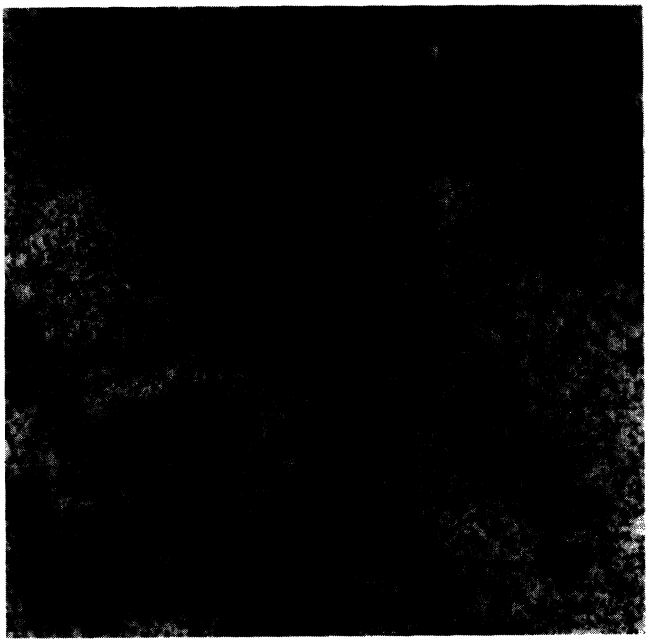

FIG. 2. Polygonization effect in a single domain with ~30 vol% 2:1:1. The grain boundary indicated by A is sharp, in contrast to that at the left-hand side of letter B. Scale bar 50 μm.

crocracks is ~1 μm but depends on the 2:1:1 precipitate size. No large scale microcracks were observed in quenched as-solidified samples, independently of the concentration of 2:1:1 precipitates.[20] This indicates that large scale microcracks in our directionally solidified composites, when present, develop as a result of the anisotropic contraction of the orthorhombic phase of 1:2:3, rather than from the growth mechanism. Moreover, comparison between Figs. 1 and 2 indicates that increasing the concentration of the 2:1:1 phase, the average size of precipitates is drastically reduced down to ~0.1–3 μm. A further distinctive feature between both samples, is that the single-domain region shown in Fig. 2 displays inhomogeneous extinction under polarized light (hereafter referred to as polygonization[40]), which results from slight misorientations between subgrains. Polygonization appears to be a distinctive feature of samples free of large scale microcracks, and could develop either during solidification, in order to accommodate internal stresses, or during the oxygen uptake process.

In contrast to these observations, the microstructure of melt-processed samples reported so far, has been described in terms of the stacking of platelets along the *c* axis.[16,18] It was argued that this platelet structure results from the much higher growth rate along ⟨110⟩ than along [001] directions of the 1:2:3 phase.[16,18] In particular, gaps between adjacent platelets containing entrapped solidified melt, were claimed to result from the interaction of the fronts of fast growing *a-b* platelets with the 2:1:1 particles present in the melt, in analogy with a dendritic growthlike mechanism.[16,18,19] Furthermore, this growth mechanism was suggested to be responsible for the creation of low angle grain boundaries between adjacent platelets.[42] It is worth mentioning that polygonization has not been described for these previously reported samples. Polygonization is a mechanism by which the elastic stress of a bent crystal is relieved through the creation of new interface area between slightly misoriented regions by dislocation migration from the center to the boundary of the new subgrains.[40] When the microstructure is composed by a stack of platelets, however, the increased interface area between them constitutes a means by which internal stresses can be relieved without the need of polygonization. This would explain the absence of polygonization in samples consisting of a stack of platelets (see Fig. 1).

Since polygonization is governed purely by interfacial energy considerations, the geometry of low angle grain boundaries needs not to be the same as that described above for microstructures consisting of a stack of platelets along the *c* axis.[43] A full study of the topological arrangement of subgrain boundaries in polygonized samples will be reported elsewhere, but the simple observation of optical micrographs (Fig. 2) suggests that they have a wide orientation distribution, at least compared to *a-b* platelet boundaries, and that they are not topologically connected.

Turning to Fig. 2, we may observe that the change in extinction across subgrain boundaries appears either sharp or gradual. Examples of both types of boundaries are indicated in the micrograph with the letter A for sharp and B for gradual boundaries. An example of a TEM image of a sharp low angle grain boundary is presented in Fig. 3. The zone axis of the image corresponds to the [001] direction and the grain boundary is nearly pure 5°—[001] twist as evidenced by the SAD pattern measured across the grain boundary, shown in the inset.

The micrograph presented in Fig. 3 also shows several dislocations preferentially oriented along [100], as expected from the easy-glide system, ⟨100⟩(001) [and ⟨110⟩(001)] determined for the 1:2:3 compound.[44] The dislocations seem to be generated from the low angle grain boundary, in agreement with the dislocation behavior observed in single crystals.[45] Moreover, the trajectories of the dislocations appear to be either unaffected or changed across the twin boundaries. For the first case, one would expect that the dislocations nucleate above the tetragonal-to-orthorhombic (T-O) transition temperature. This situation would correspond to an alternate orientation of the Burgers vector along [100] and [010], as found in single crystals.[45] Conversely, other dislocations, arrowed in the micrograph, behave as being pinned by twin boundaries. In this case, the dislocation is observed to bow out between pinning points, as first described by Rabier and Denanot.[44] The region displayed in Fig. 3 also appears highly strained. The strain is reflected as severe bending of twin boundaries along the [110] direction. In addition, contrast fringes parallel to the twin boundaries can be observed. Since depth fringes associated with twin walls are not expected for images viewed along [001], these are probably related to lattice bending along the [001] direction. The dislocation density in

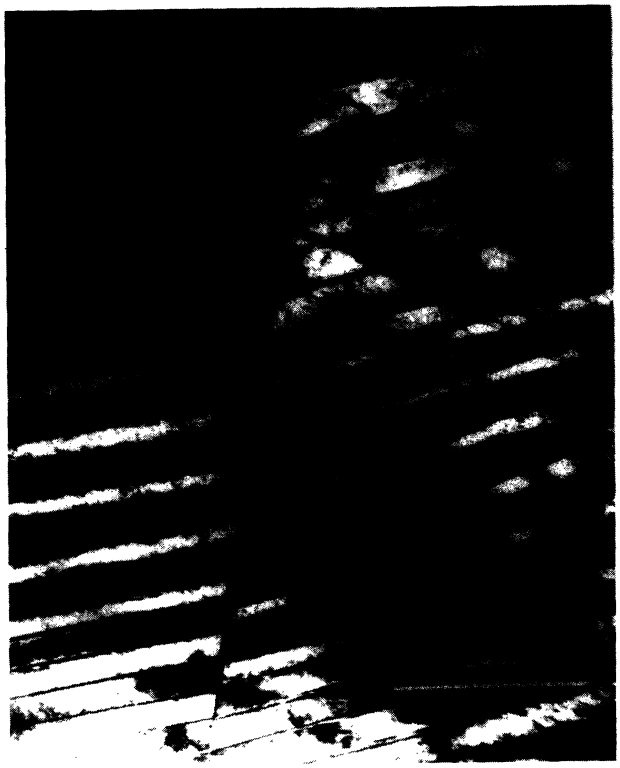

FIG. 3. TEM image viewed along the [001] direction showing a nearly pure 5°−[001] twist boundary. Note that several dislocations originate from the grain boundary. The inset presents the SAD pattern obtained across the boundary. Scale bar represents 0.5 μm.

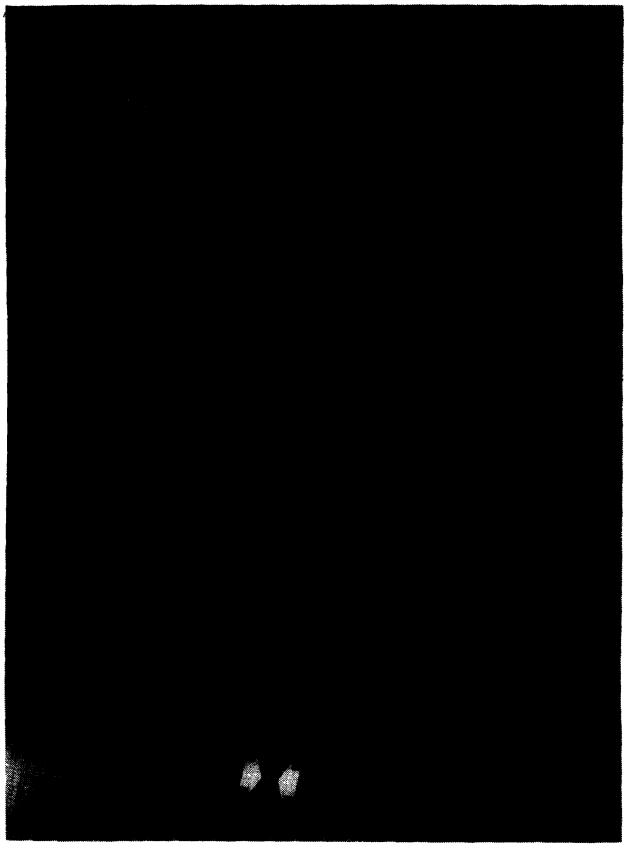

FIG. 4. HRTEM image viewed along the [100] direction showing a transition from a well-ordered zone (left-hand side) to a highly defective one (right-hand side of the micrograph) in the 1:2:3 matrix along its associated SAD patterns. Distance between arrow tips equals 1.17 nm.

such areas was estimated $\sim 10^9$ dislocations/cm^2, one order of magnitude lower than that reported in other melt-processed samples.[37,39] This density may be locally increased around 2:1:1/1:2:3 interfaces, but this increase has all times a local character.

Besides sharp low angle grain boundaries, gradual variations of optical extinction under polarized light as those marked with B in Fig. 2, suggest a gradual accommodation of lattice misorientations. Stress effects associated with the matrix bending necessary to connect misoriented subgrains is likely to be a driving force for the nucleation of lattice defects, such as planar faults. Indeed, the density of stacking faults has been found to increase dramatically at particular places. Figure 4 shows a high-resolution TEM (HRTEM) micrograph viewed along the [100] direction displaying the transition from a well ordered region to a highly defective one. The left-hand side of the micrograph shows a nearly undisturbed 1:2:3 matrix along with its associated SAD pattern; diffraction spots associated to this side appear well defined. Lattice fringes undergo intensive bending towards the upper part of the micrograph. Note that the (00l) diffraction spots shown in the inset corresponding to this highly defective side are practically indistinguishable from each other due to intense diffuse streaking along the c axis thus signaling that the lattice lacks a well defined periodicity along this direction. The observation of locally bent areas between subgrains, as inferred from the gradual extinction zones shown in Fig. 2, provides a possible explanation for the lateral fault density gradient observed in Fig. 4. Gradual extinction reveals indeed the existence of nonpolygonized, continuously bent, zones having a finite curvature. Hence, clustering of stacking faults at some regions could be interpreted as mechanism with which to accommodate this bending.

It is worth mentioning that in 2:1:1 free areas within subgrains found in samples with ~ 15 vol % 2:1:1, stacking faults constitute a generalized defect. Stacking faults have been reported to be a common defect either in 1:2:3 ceramic powder,[46,47,52] thin films,[48,49] and melt-processed samples.[50,51] Commonly observed stacking faults consist of an extra CuO chain layer giving rise to a local double-chain layer or 1:2:4 structure.[52] Each fault is bounded by two partial dislocations with displacement vectors $+/-[a/2,0,c/6]$ and $[0,b/2,c/6]$ alternating across the twin boundaries.[46,40] Figure 5 shows a typical TEM image corresponding to the [3 −6 1] zone axis of a 2:1:1 free region in a ~ 15 vol % 2:1:1 sample displaying a high density of stacking faults, shown perpendicular to the twin boundaries in the micrograph. The faults are inclined to the plane of the foil and therefore display depth

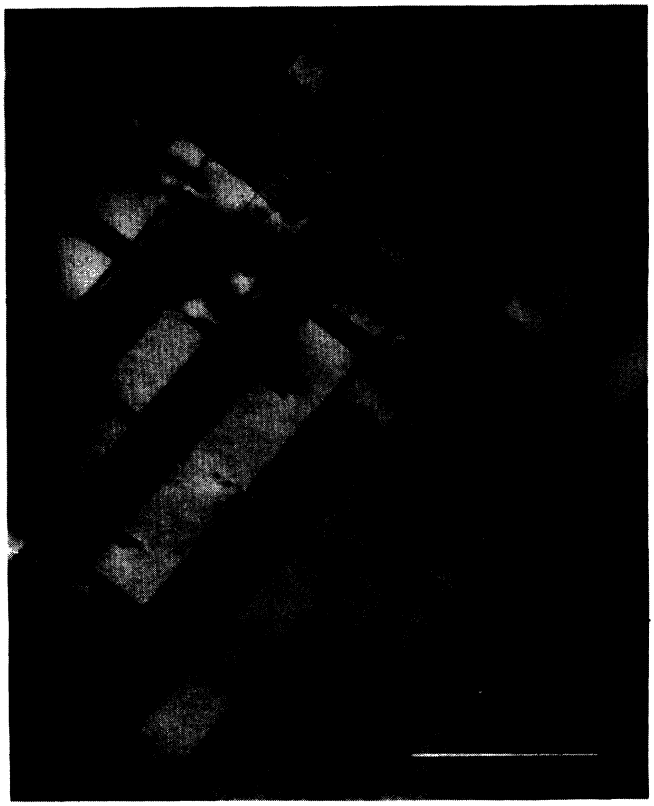

FIG. 5. TEM image viewed along the [3 −6 1] direction of a 1:2:3 matrix region in a sample with 15 vol % 2:1:1 displaying twin boundaries and stacking faults. Scale bar corresponds to 0.25 μm.

FIG. 6. Lattice fringe image corresponding to the [100] zone axis of a region close to that shown in Fig. 5. Note the high density of stacking faults. Scale bar corresponds to 25 nm.

fringes. Figure 6 is a lattice fringe image of the same region shown in Fig. 5 viewed along the [100] zone axis. It is observed that lattice fringes in the vicinity of the partial dislocations bounding the stacking faults are bent to accommodate the extra CuO layer; depending on the local fault density the strain generated may extend up to several unit cells above and below the plane of the fault. Because of the variable stacking sequences along the *c* axis, the *c* parameter measured at different places was found to have variable values comprised between the corresponding ones to the pure 1:2:3 and 1:2:4 phases.

The observations made above suggest that the increased fault concentration found in some matrix regions is governed by the stress field which develops upon the T-O transition and because of the anisotropic contraction of the 1:2:3 phase when cooled from high temperatures. The formation of CuO stacking faults requires the availability of Cu in excess relative to the nominal 1:2:3 stoichiometry. Local Cu excess may result from a tendency of the 1:2:3 phase for decomposition during, e.g., oxygen annealing,[53] or, alternatively, could be incorporated during solidification from a CuO-rich melt as impurity. Just below the peritectic temperature, where growth takes place in directional solidification or melt-texturing experiments, the 1:2:4 phase is unstable in air,[54] thereby preventing the long-range ordering of the 1:2:4 phase into separated domains. Moreover, after solidification, for temperatures below the peritectic and compositions where there is intimate intermixing of 1:2:3 and 1:2:4 faults, it has been claimed that strain considerations are likely to inhibit the segregation of the 1:2:4 polytype as a separate phase.[48]

The above considerations on the occurrence of stacking faults in matrix regions free from 2:1:1 precipitates indicate that there is an inherent tendency of 1:2:3 grown directionally from the melt for their formation. In the case of melt-textured samples, the origin of such stacking faults has not been yet ascertained. However, Cu-excess incorporation into the growth front during the solidification process seems a likely mechanism. Subsequent lateral motion of stacking faults along the *a-b* planes is expected to be governed by the stress resulting from the T-O transformation and the anisotropic contraction of the matrix when cooled. As a result of this motion, clustering of stacking faults may occur in places as that shown in Fig. 4 to give a highly defective area where the lattice may even lose a well-defined periodicity along the *c* axis.

B. Effect of 2:1:1 additions

The effect of 2:1:1 excess additions on the microstructure is manyfold. First, there is a size effect such that when the concentration of 2:1:1 is increased, the average size of the precipitates is decreased. This effect was illustrated above by comparing Figs. 1 and 2. The important consequence of this behavior is that 2:1:1 additions result

in a drastic increase of the effective 2:1:1/1:2:3 interface area. While the typical size of 2:1:1 precipitates in samples with nominal 1:2:3 stoichiometry ranges from 5 to 15 μm, this size is reduced down to 0.1–3 μm when there is a 2:1:1 concentration of about 30 vol %. This size reduction effect can be accounted for by considering that any 2:1:1 excess in the semisolid melt increases the number of nucleation sites for 2:1:1 released during the 2:1:1 + liquid → 1:2:3 peritectic reaction, thereby inhibiting their subsequent growth.[42] Also important is the fact that we did not find appreciable variation of the precipitate size along the processed bars. Taking into account the fact that the residence time in the liquid of 2:1:1 particles located in the top and the bottom of the bars differs by about 100 h, this means that particle coarsening by Ostwald ripening is saturated after a relatively short time. The most noticeable consequence of increasing the effective 2:1:1/1:2:3 interface area is the development of local complex defective structures adjacent to the 2:1:1 boundaries, to be analyzed below.

Figure 7 shows a region containing several precipitates viewed along [100] of a sample containing ~30 vol % 2:1:1. It is straightforward to note that the superconducting matrix is highly strained when the concentration of 2:1:1 precipitates is high as evidenced by strain contrast, and bending of twin boundaries, visible in the region enclosed between square marks.

In addition, Fig. 7 indicates that the density of stacking faults in matrix regions rich in 2:1:1 precipitates is also high; a rough estimation, assuming a foil thickness of ~100 nm gives $\sim 10^{14}$ faults/cm^3 of average length $\sim 6\times 10^{-5}$ cm, which is of the same order of magnitude as the density found in some 2:1:1 free areas (see Fig. 5). Because of the variable stacking-fault density in 2:1:1 free regions of the matrix, we were not able to find a well-defined correspondence between stacking-fault density adjacent to and away from 2:1:1 precipitates. However,

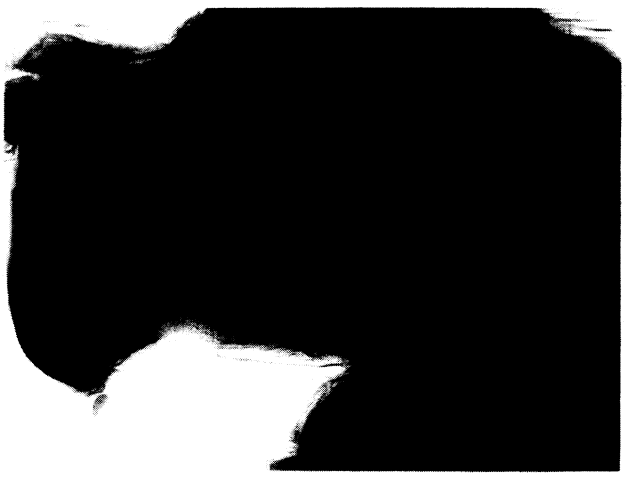

FIG. 7. TEM image corresponding to the [100] zone axis of a sample with ~30 vol % 2:1:1. The matrix between precipitates is highly defective. In particular the area enclosed between square marks contains stacking faults and twin boundaries. A microcrack which is stopped *within* a 2:1:1 precipitate is indicated by an arrow head. Scale bar corresponds to 1 μm.

there are places along the 2:1:1/1:2:3 interfaces where the stacking-fault density is locally increased. This effect has already been described by Wang, Goyal, and Kroeger in 1:2:3 thick films deposited on Ag 10% Pd substrates.[26]

Along the 2:1:1/1:2:3 interface, first we observe that the stacking-fault density is increased in places where a microcrack interacts with a 2:1:1 particle, as shown in Fig. 8(a). Microcracks form and propagate along the easy cleavage *a-b* planes preferentially after the T-O transition because the thermal contraction along the *c* axis of the orthorhombic 1:2:3 crystal lattice is larger than in the tetragonal phase. Therefore, when cooling the lattice mismatch stress created at the 2:1:1/1:2:3 interface and the stress field generated at the intercept between a microcrack and the boundary of a 2:1:1 precipitate can be accommodated by the nucleation of stacking faults parallel to the *a-b* planes. This appears to be an important stacking-fault generation mechanism in directionally solidified 1:2:3 ceramic bars. An interesting feature observed in Fig. 8(a) is that the walls of the microcracks appear highly defective, and this is a feature observed in most of microcracks. This defective layer has a thickness of about the same order as the gap of the microcrack itself, i.e., ~70 nm. The gap within the microcrack is partially filled with Cu-rich material as deduced from EDS. The existence of this defective layer together the material inside the microcrack could be related with some degree of decomposition of the 1:2:3 phase.[53]

The stacking-fault density appears further controlled by the local orientation of the 2:1:1/1:2:3 interface relative to the *a-b* planes. Figure 8(b) shows a detail of the 1:2:3 matrix adjacent to two different precipitates viewed along the [100] direction. The interfaces of the two precipitates are indicated by arrowheads. The upper left interface is nearly perpendicular to the *a-b* planes, or the planes of the faults, whereas in the lower one, the boundary is nearly parallel to the *a-b* planes. As seen in the micrograph, the boundary between 1:2:3 and the lower left 2:1:1 particle contains fewer stacking faults than the upper 2:1:1/1:2:3 boundary, where the faults form dense pileups in some regions. It can be observed in the micrographs that the length of the faults associated to the interface is shorter, $\sim 3\times 10^{-5}$ cm, than that measured above for the bulk of the 1:2:3 matrix. The faults are associated with a large amount of strain as indicated by contrast variations along their traces.

Stresses associated with the 2:1:1/1:2:3 interfaces can arise from two different mechanisms. The first takes into account the thermal expansion and elastic modulus mismatch between the two phases.[36] Secondly, stress is thought to result from the incorporation of 2:1:1 decomposition products into the 1:2:3 matrix. Below the peritectic temperature, there is a thermodynamical driving force for solid-state dissolution of 2:1:1 precipitates embedded in the 1:2:3 matrix. As 1:2:3 is a line compound with fixed-cation stoichioimetry, 2:1:1 dissolved species cannot be easily accommodated into the matrix unless defects are formed. In addition, the transformation of 2:1:1 into 1:2:3 in accompanied by a strong volume reduction. Precipitate dissolution is likely only to occur whenever the energy associated with defect formation is lower than

the excess free energy of the 2:1:1 phase below the peritectic temperature; therefore stacking faults associated with 2:1:1/1:2:3 interfaces probably are formed at relative high temperatures. Our observations seem to indicate a strong correlation between stacking-fault density and matrix orientation, i.e., this density always increases when the interface is perpendicular to the *a-b* planes, while the correlation between stacking-fault density and curvature of the interface[26] is not so apparent in our samples. This observation agrees with the fact that *a-b* planes normal to the interface provide an easy channel for diffusion of Y_2O_3 and BaO into the 1:2:3 matrix. Since the thermal contraction of the 1:2:3 lattice is significantly higher along the *c* axis, a tensile stress state is created between *a-b* planes which is likely to facilitate this process. Furthermore, the shorter length of stacking faults originating at 2:1:1/1:2:3 interfaces compared with those present in the bulk matrix, support the idea that the former are formed by a distinct generation mechanism.

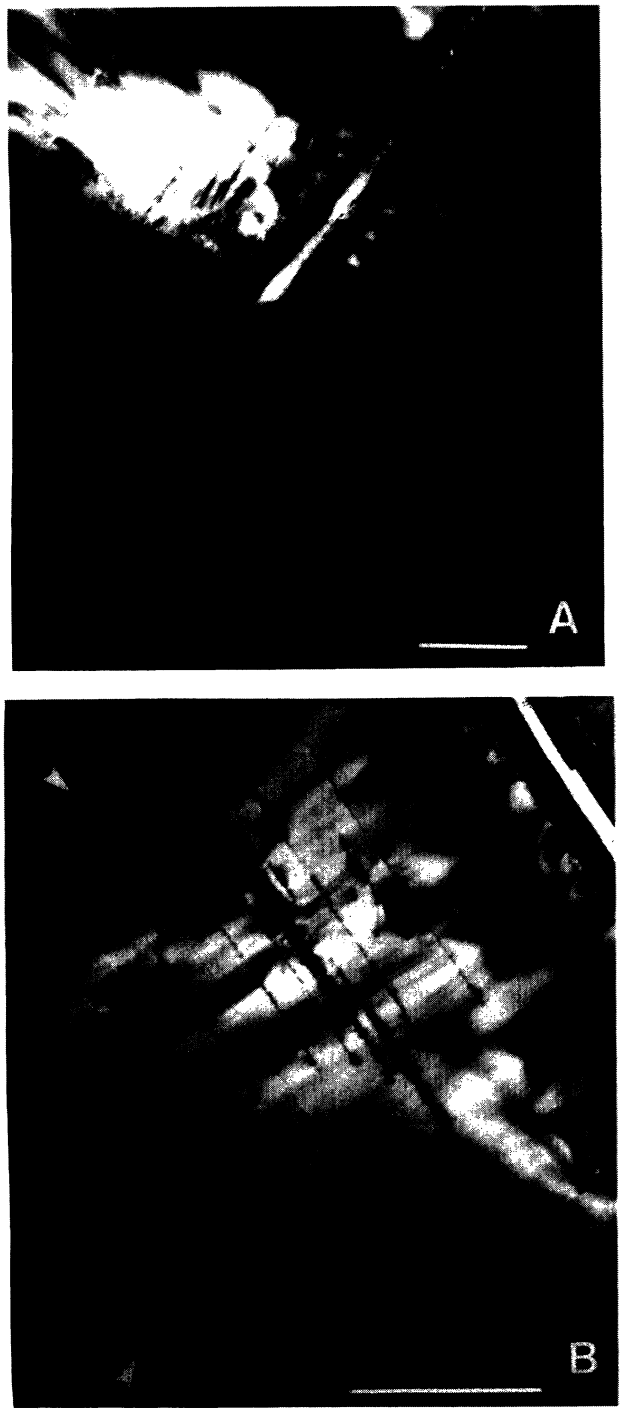

FIG. 8. Stacking faults associated to the interaction of a microcrack and a 2:1:1 precipitate (A), and a 2:1:1/1:2:3 interface nearly perpendicular to the *a-b* planes (B). Both images viewed along [100] direction. Scale bars represent 0.5 μm.

The dissolution of 2:1:1 to give 1:2:3 may be tentatively approximated by $Y_2BaCuO_5 \rightarrow (\frac{1}{3})YBa_2Cu_3O_{6.5} + (\frac{5}{6})Y_2O_3 + (\frac{1}{3})BaO$. Taking into account the above considerations, the only mechanism by which local dissolution of 2:1:1 can be accommodated into the 1:2:3 lattice would be the insertion of extra Y_2O_3, and to a lower extent, BaO layers. The observation of a yttrium-enriched thin layer adjacent to 2:1:1 boundaries[26] gives further confidence to the above mechanism. Conclusive evidence for the above model, however, would come from the investigation of the chemical nature of the stacking faults associated with the 2:1:1/1:2:3 interfaces. Ledges on 2:1:1 facets have also been observed on a few precipitates,[26] and attributed to a variation in size of 2:1:1 precipitates after entrapment in 1:2:3. Such ledge structures were only observed associated to facets terminating with a (001) plane of the 1:2:3 matrix; therefore the ledge front was always normal to the *a-b* planes. This feature in combination with the existence of a yttrium-enriched layer, would be considered as evidence for an alternative mechanism of 2:1:1 dissolution along interface orientations parallel to the *a-b* planes of the surrounding 1:2:3 matrix. Contrary to this interpretation, such ledge structures were considered as evidence for the local growth of 1:2:3 at expense of 2:1:1 precipitates along the facets, assisted by the supply of Cu and Ba-rich phases from closely located platelet boundaries.[26] However, this mechanism would require gap terminations to occur along *a-b* planes intersecting the ledge front at a short distance, otherwise Cu and Ba cations would have to diffuse across the *a-b* planes to feed the reaction zone at the interface. Since diffusion of Ba along the *c* axis is at least three orders of magnitude slower than diffusion in the *a-b* plane,[55] the latter possibility appears rather unlikely. In fact, such gaps terminations near ledge fronts were not observed and therefore the interpretation of such ledge structures remains an open question. The post-solidification 2:1:1/1:2:3 interfacial processes constitute the key for the understanding of the structural and chemical nature of these interfaces, and their elucidation deserves further attention. In order to gain further insight into interfacial processes, we are currently investigating the effect of aging on the microstructure of our composites.

TEM observations of the 2:1:1/1:2:3 interfaces also gives further insight into the effect of 2:1:1 precipitates against cracking. As described previously in this work, when the average size of the 2:1:1 precipitates is reduced,

large scale cracks are completely suppressed and only short-range microcracks remain. SAD patterns obtained at either side of microcracks indicated that the crystallographic misalignment of the matrix rarely exceeds 1°, in agreement with previous investigations.[16] The main conclusions about the mechanical properties of 1:2:3-2:1:1 composites may be drawn from the indentation investigations by Goyal *et al.*[36] and Fujimoto, Murakami, and Koshizuka.[56] In brief: 2:1:1 precipitates behave as rigid particles in a brittle material. Microcracks in the 1:2:3 matrix propagate along the easy (001) cleavage planes (or *a-b* planes). The mechanical performance of the composite is governed by a complex interplay between anisotropic interfacial strengths, and thermal and elastic differences between the two phases. The average thermal-expansion coefficient between 20 and 900 °C of 1:2:3 is about 1.7×10^{-5} K^{-1}, somewhat higher than that of 2:1:1, about 1.24×10^{-5} K^{-1}. However, the thermal contraction of 1:2:3 is higher along the *c* axis, perpendicular to the cleavage planes. In this situation cracks are expected to intersect the 2:1:1 particles, and this is the tendency we have observed in most of the precipitates. The microcracks actually stop *within* the 2:1:1 precipitate generating an intense strain field around their terminations, as illustrated in Fig. 8(a).

Figure 9 shows a 2:1:1 precipitate intercepted by a microcrack extending across the 1:2:3 matrix at the two points arrowed in the micrograph. The small inclusions embedded within the 2:1:1 precipitate were identified as Y_2O_3 using electron-energy-loss spectroscopy and their origin is discussed elsewhere.[20] It may be clearly observed that both intercepts are associated with strain contrast and a complex dislocation structure within the precipitate. In particular, a lens-shaped region displaying several dislocations and depth fringes nearly parallel to the prolongation of the microcrack, extends from the lower left intercept and divides the 2:1:1 precipitate into two halves with distinctive contrast. Note that several dislocations end at the upper boundary generating a stress field around their terminations. The defective zone separating both halves of the 2:1:1 precipitate corresponds to a grain boundary, inclined to the foil normal as demonstrated by the observation of inclination fringes, which nearly coincides with the line joining both intercepts of the microcrack with the precipitate. This case constitutes an interesting example of the behavior of 2:1:1 precipitates against cracking. The microcracks develop at high temperature during the cooling and oxygen-anneal steps as a result of the anisotropic contraction of the matrix. Therefore, the 2:1:1 particles are likely to be influenced by a persistent tensile radial stress field around them at temperatures above room temperature, which would result in severe plastic deformations within the precipitates. We can conclude that 2:1:1 precipitates act as crack stoppers, enhancing thereof the fracture toughness of the composite, in agreement with indentation investigations performed on other melt-processed samples.[36,56] Since increasing the concentration of 2:1:1 in the composite also decreases the size of the precipitates, the final result consists of a very pronounced increase of the interface area. Thus, the stress state, and the defects accompanying it, are accommodated within a larger effective volume of the 1:2:3 matrix.

FIG. 9. TEM image of a 2:1:1 precipitate intercepted by a microcrack at places arrowed in the figure. The region between both intercepts shows a complex dislocation network. The arrowhead indicates Y_2O_3 inclusions. The scale bar corresponds to 0.5 μm.

C. 2:1:1/1:2:3 interfaces

The microscopic capture mechanism of 2:1:1 particles by an advancing 1:2:3-liquid interface is important because it controls the microstructure of the 2:1:1/1:2:3 interface before subsequent modifications induced by chemical and mechanical interactions between the 2:1:1 precipitates and the 1:2:3 matrix, discussed above. In turn, the nature of this interface is of considerable current interest because it is thought to play a fundamental role in flux pinning.

Figure 10 shows a TEM micrograph where 2:1:1 precipitates with different sizes embedded in a highly defective matrix are observed. The volume percentage of the 2:1:1 phase in this sample is estimated to be ~30%. Examples of SAD patterns obtained across some 2:1:1/1:2:3 interfaces are shown in Fig. 11. Indexation of the patterns was aided by the calculation software "diffract 1.5a ."[57] Interestingly, SAD patterns indicated parallelism between crystallographic directions of precipitate and matrix. In general, alignment between particular directions was more frequently observed, the smaller the size of the precipitates, and the orientation relationship changed from precipitate to precipitate. For instance,

FIG. 10. TEM image of a region containing several precipitates with different sizes. The relative orientations of precipitates 1–4 were determined. The scale bar corresponds to 1 μm.

orientation relations deduced for precipitates 1 to 3 indicated in Fig. 10, are $1{:}[100]_{1:2:3}\|[-261]_{2:1:1}$, $(001)_{1:2:3}\angle(412)_{2:1:1}(3.4°)$ [Fig. 11(a)] $2{:}[100]_{1:2:3}\|[13-3]_{2:1:1}$, $(001)_{1:2:3}\angle(301)_{2:1:1}(3.5°)$, $3{:}[100]_{1:2:3}\|[-102]_{2:1:1}$, $(001)_{1:2:3}\angle(211)_{2:1:1}(1.7°)$ [Fig. 11(b)], where the angles indicate the misorientation between the corresponding planes (rotation around the zone axis). For the bigger precipitate, no evidence for a particular orientation was found within the rotation range allowed by the microscope. Figures 11(c) and 11(d) show examples found for matrix orientations other than $[001]_{1:2:3}$, (c): $[-120]_{1:2:3}\|[23-2]_{2:1:1}$, $(001)_{1:2:3}\angle(101)_{2:1:1}(34°)$, (d): $[1-11]_{1:2:3}\|[0-21]_{2:1:1}$, $(-112)_{1:2:3}\angle(100)_{2:1:1}(7°)$.

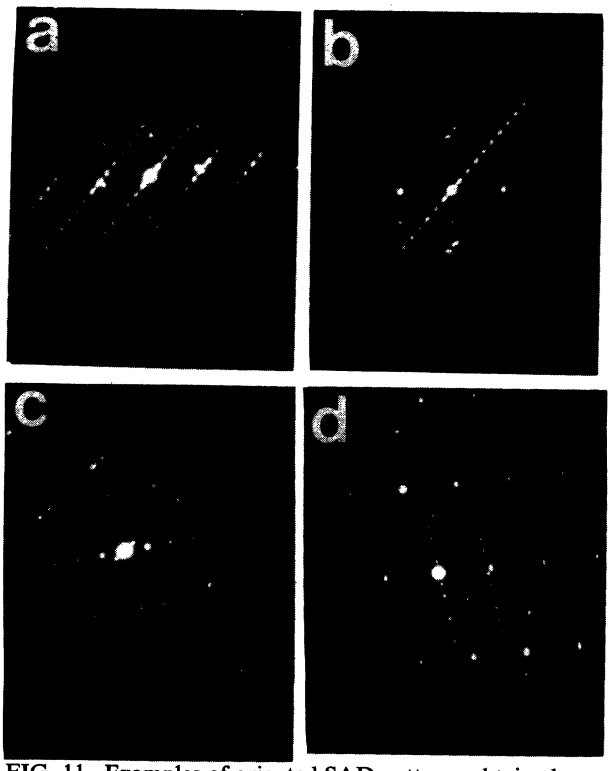

FIG. 11. Examples of oriented SAD patterns obtained across different 2:1:1/1:2:3 interfaces. The four patterns manifest parallelism between particular directions of precipitate and matrix.

In order to obtain conclusive insights into the possible occurrence of texture in the 2:1:1 phase embedded in the aligned 1:2:3 matrix, we measured the room-temperature ESR spectra of a 1:2:3-2:1:1 single domain containing ~30 vol% 2:1:1 for different 1:2:3 sample orientations relative to the applied magnetic field. Cu ions in 1:2:3 at room temperature are silent in the ESR experiment because of the strong antiferromagnetic correlations,[58] while 2:1:1 is an anisotropic paramagnet with $g_{\|}=2.222$ and $g_{\perp}=2.072$.[59] Therefore, comparison between room-temperature ESR spectra recorded at different sample orientations is a sensitive way to obtain information on the preferential orientation effects. We were unable to detect any anisotropic behavior in our 1:2:3-2:1:1 composites. Both intensity and location of the ESR peaks were undistinguishable for any crystal orientation. Therefore we can conclude that 2:1:1 precipitates embedded in the 1:2:3 matrix are not textured in our directionally solidified samples.

In contrast with this result, investigations on samples textured by a "liquid extraction" method, which uses a substrate as liquid sink,[60] evidenced some anisotropy of the ESR spectra.[61] A preferential orientation of 2:1:1 precipitates relative to the 1:2:3 matrix might be favored in the situation where 1:2:3 nucleates and grows from a 2:1:1 particle. In the case of 1:2:3 growing on Y_2O_3 substrates, the CuO-rich liquid reacts with the substrate to form a 2:1:1 enriched interface,[60] such that subsequent nucleation of 1:2:3 is likely to be determined by the orientation of the 2:1:1-liquid interface.[60] This mechanism would explain the anisotropic orientation distribution of 2:1:1 observed by Pellerin.[61] On the other hand, for 1:2:3 growing directionally from the melt, the particle engulfment process is governed by a complex interplay between kinetic and interface energy considerations, namely: velocity of the advancing interface, melt viscosity, and particle size. According to early investigations by Uhlman, Chalmers, and Jackson,[41] two situations can be distinguished for which a solid particle can be engulfed by an advancing solid-liquid interface, namely, (i) when $\sigma_{ps}<\sigma_{pl}+\sigma_{ls}$ (σ_{ps} is the interfacial energy between a particle and the advancing interface, σ_{pl} is the interface energy between a particle and the liquid, and σ_{ls} is the interface energy between the liquid and the advancing interface) the particle can wet the interface and is entrapped; (ii) when $\sigma_{ps}>\sigma_{pl}+\sigma_{ls}$ the particle is pushed by the advancing interface into the liquid. These considerations are valid for particle sizes below a critical radius, r_c. Conversely, when $r>r_c$, the particles will be entrapped regardless the balance of interface energies involved. For anisotropic materials, such as 2:1:1 and 1:2:3 crystals, we can expect the above process to be governed by a complex interplay between orientation and size of the parti-

cles. These considerations suggest that the incorporation of 2:1:1 particles into the bulk 1:2:3 would be favored for particular orientations if the growth rate parallel to *a-b* planes, radius of the particles and melt viscosity were appropriate. A particle with $r < r_c$ would either be pushed until it adopts a favorable orientation (assuming a near spherical particle being pushed free to rotate in the liquid), or coarsen in the liquid until being engulfed. On the other hand, particles with $r > r_c$ would be entrapped regardless of their orientation. Unfortunately, relevant parameters governing the process are unknown. Furthermore, the capture mechanism is likely to be more complicated because of constitutional supercooling effects arising from the concentration gradient of solute created ahead of the growth front by dissolving 2:1:1 particles.

Our microscopic observations suggest that 2:1:1 particles tend to optimize the lattice matching with the growth front before being definitively engulfed, though the relevant parameters governing the engulfment process do not allow the development of a preferential orientation. We have indeed observed that 1:2:3/2:1:1 interfaces are sharp and undisturbed on the atomic scale. An example of this is shown in the HRTEM micrograph of Fig. 12. The image shows the undisturbed interface between a ~ 0.7-μm precipitate and the 1:2:3 matrix. The orientation between both crystals was found to be $[331]_{1:2:3} \| [-211]_{2:1:1}$, $(01-3)_{1:2:3} \angle (01-1)_{2:1:1} (6.5°)$. Parallel moiré fringes result from the local superposition of both undisturbed crystal lattices. On this scale, no correlation between proximity to the interface and lattice defect density was observed. Small dislocations in the matrix away of the interface are indicated by arrowheads.

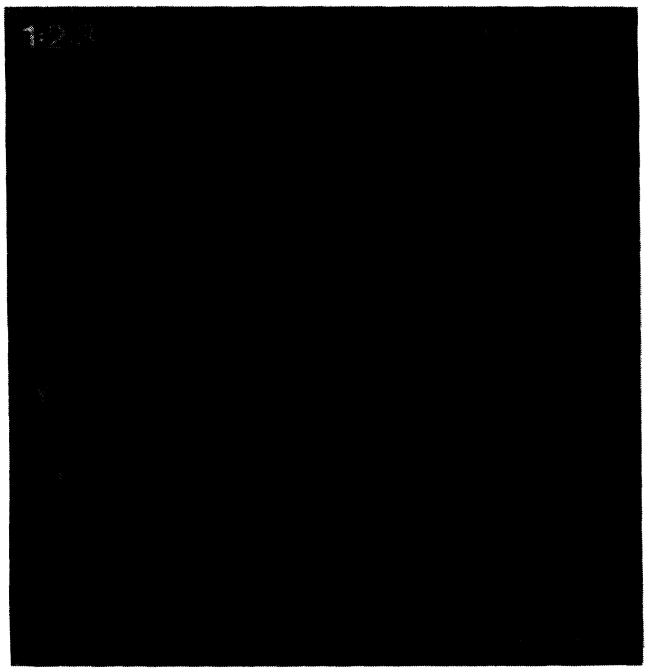

FIG. 12. HRTEM image of a 2:1:1/1:2:3 interface. The zone axes are [331] and [−211] for 1:2:3 and 2:1:1, respectively. Arrowheads indicate small dislocations. Scale bar corresponds to 4 nm.

The observations given above indicate that 2:1:1/1:2:3 interfaces are inherently sharp and undisturbed on the atomic scale, in agreement with previous observations on MPMG samples.[34,35] Once solidification has been completed, defects are formed as a result of subsequent thermal cycling. During cooling, thermal-expansion mismatch between 2:1:1 and 1:2:3 and the interaction of microcracks with precipitates causes stresses at the interface which are relieved through the nucleation of stacking faults where the 2:1:1/1:2:3 interface is normal to the *a-b* planes, leaving the interface segments between fault agglomerations apparently undisturbed on the atomic scale. Stacking faults are likely to accommodate decomposition products of the 2:1:1 precipitates. Although there is yet no direct chemical evidence for such a mechanism, the observation of a yttrium-enriched layer around precipitates[26] supports the idea that where the formation of stacking faults is energetically unfavorable due to matrix orientation effects, the precipitate decomposition can be locally accommodated by generation of numerous point defects. It turns out then that most of the defects associated to the 2:1:1/1:2:3 interface are generated during thermal cycling after solidification. We believe that these considerations would enable us to set controlled defect engineering of 2:1:1/1:2:3 interfaces through systematic studies of thermal treatments and processing conditions.

D. Implications on critical currents

One of the main concerns in the study of melt-processed 1:2:3 superconductors is to determine which defects have an important contribution to the flux pinning in these materials. Our present work has confirmed that sharp interfaces at the atomic scale occur between 1:2:3 matrix and 2:1:1 precipitates; thus a high gradient of the superconducting order parameter must be expected and so an intense pinning force must be originated at these interfaces.[28,32] It is a complex matter, however, to determine under which conditions 2:1:1 precipitates are the dominant pinning centers. A full quantitative analysis of the magnetic-field and temperature dependence of critical currents in samples having different concentration of well characterized 2:1:1 precipitates is required to ascertain when this pinning mechanism is dominating.[33] It is also straightforward to recall that a strong orientation dependence of the different pinning mechanisms is expected to occur in 1:2:3 and thus the dominance or not of a pinning mechanism will also depend on the field orientation.

In the sample with 30 vol % 2:1:1 studied in this work the concentration of 2:1:1 precipitates has been found to be much higher and more homogeneously distributed than any other matrix defects such as stacking faults or dislocations which could also contribute to the overall flux pinning. Within the scope of the single vortex pinning regime and, as long as the vortex separation is high enough, vortices may be pinned at the 2:1:1/1:2:3 interfaces. We have indeed recently demonstrated that our composite textured ceramics have inductive critical current at fields below ~ 1 T which are proportional to

V/d, where V is the 2:1:1 phase volume fraction and d is its mean particle diameter.[33] This rule was found to be valid both when $H\|c$ and $J_c^{ab}(H\|c)$ is measured and when $H\|ab$, where the irreversible magnetization of the hysteresis loops is dominated by $J_c^c(H\|ab)$. In both cases, however, the Lorentz force is directed parallel to the *a-b* planes and so the critical currents will not be dominated by defects lying parallel to the *a-b* planes. Moreover if the 2:1:1/1:2:3 interface is the dominating pinning center we should have $J_c^{ab}(H\|c)\propto\xi_{ab}(V/d)$ and $J_c^c(H\|ab)\propto\xi_c(V/d)$,[28,32] i.e., $J_c^{ab}/J_c^c\sim\xi_{ab}/\xi_c\sim 7$. The experimentally observed ratio is indeed very near to this prediction and thus we have a further indication of the dominance of interfacial pinning in our samples at low magnetic fields. Now, within the scope of the single vortex pinning regime, when the magnetic field increases and the flux-line lattice parameter decreases, pinning by 2:1:1/1:2:3 interfaces may become ineffective because the relatively high separation between 2:1:1 particles would not allow the pinning of all the vortices. After this crossover magnetic field other defects occurring near the interface or within the 1:2:3 matrix, such as dislocations, stacking faults, and microcracks, may start to have some relevance as well in the observed critical currents. As we have pointed out above, the concentration of these defects has been found to be relatively high in our 1:2:3-2:1:1 composites so they could contribute to the observed critical currents at high fields. A full analysis of the different vortex pinning regimes will be reported elsewhere,[33] but for the time being we may suggest that there is no real controversy about the point of dominance of interface pinning or pinning by defects associated with the interfaces in these composite ceramics because they could become dominant pinning centers at different magnetic-field regimes.

Dislocations[24] and stacking faults[26] have been suggested to be the dominant flux-pinning centers in melt-processed 1:2:3. The former have been found to correlate nicely with an increase of J_c,[24] even if it is not yet known how effective they are as pinning centers in presence of a high concentration of 2:1:1 small precipitates, i.e., it would be very appealing to investigate how the different defects interact among themselves. Stacking faults, instead, will probably not contribute too much to the overall pinning when $H\|c$ because there is a small volume of interface between the matrix and their lateral terminations. Only in the $H\|ab$ configuration is this volume important but then there is a tendency to mix up this pinning force with other defects also lying parallel to the *a-b* planes and the intrinsic pinning mechanism. In this work we have shown that the stacking-fault density near the 2:1:1/1:2:3 interfaces and within the 1:2:3 matrix is similar, even if the distribution is quite inhomogeneous with a local increase of its density in some regions where polygonization occurs. Overall, however, there is not a clear increase of their density when a higher concentration of 2:1:1 precipitates is introduced in the 1:2:3-2:1:1 composite. Moreover, as it has been shown,[52] the structure of stacking faults consists of a double chain between CuO_2 planes, i.e., the crystal structure of the superconducting phase 1:2:4. Therefore, only a small decrease of the superconducting condensation energy occurs locally with this defect, even if we take into account the associated strain; therefore it's very unlikely that the observed enhancement of the critical current at low magnetic fields in the 1:2:3-2:1:1 composite may be associated with the stacking faults observed in our TEM micrographs.

In analogy with stacking faults, microcracks could also have some relevance in the critical current of 1:2:3-2:1:1 superconducting composites because they can behave either as active flux-pinning defects or as current limiters. Microcracks could have a higher contribution to flux pinning when the vortices are directed parallel to the *a-b* planes, because the overlapping volume of the vortices and the defect is bigger in this direction. As compared to stacking faults, however, a higher gradient of the order parameter should be expected in this case thus increasing the interfacial pinning force. Our samples show a progressive reduction of the length and width of the microcracks directed parallel to the *a-b* planes for higher concentrations of 2:1:1 but their density increases. It's not possible then to disregard that some interfacial pinning occurs at high fields in these small microcracks and their strongly defective layer. Otherwise, microcracks could also behave as current limiting defects when currents flow along the *c* axis. However, due to the limited effective cross section covered by these defects (and the fact that the whole sample consists of interconnected single-domain material), when the concentration of 2:1:1 precipitates is high, it's very unlikely that transport critical currents flowing perpendicular to the *a-b* planes are actually limited by microcracks. This is, however, a point which deserves further experimental investigation.

Finally, other defects observed in our directionally solidified 1:2:3-2:1:1 composites, such as twin boundaries and low angle grain boundaries, have only minor contributions to flux pinning. The effectiveness of twin boundaries as pinning centers when the Lorentz force crosses the {110} planes was first demonstrated by magnetoresistance measurements,[22] however the relevance of this defect in the critical currents of 1:2:3-2:1:1 composites has been found to be relatively low by measuring the irreversible magnetization when the magnetic field rotates within the *a-b* plane.[21] Only minor enhancements of ΔM and thus $J_c^c(H\|ab)$ were observed when the magnetic field crosses {110} planes, thus meaning that other terms dominate J_c, particularly interface pinning with 2:1:1 precipitates. The concentration of twin boundaries in our directionally solidified materials were found to be very similar to those reported by these authors, thus we may infer that these defects will not be dominant in this case either.

The direct contribution to critical currents of sharp low angle grain boundaries, their associated dislocations, and the strain fields observed when polygonization occurs is very difficult to assess because it is not possible to modify independently their concentration. Nevertheless, the observation in our samples of critical currents above those observed in 1:2:3 single crystals suggests that even if low angle grain boundaries have a weak-link character, their topological distribution within the single domains do not force them to behave as current limiting defects.

We must remark in any case that all the observed sharp low angle grain boundaries had misorientation angles below about $\sim 5°$ and J_c is reduced only by a factor of 2–3 in this case.[62] Now concerning the strain fields associated to the highly defective regions existing when a smooth accommodation of texture by polygonization occurs, it cannot be disregarded that they have an additional contribution to flux pinning. Nevertheless, this contribution must be limited because of the low concentration of these defects as reflected by optical microscopy and TEM. They could manifest at most as a source of large scale inhomogeneous pinning.

IV. CONCLUSIONS

The microstructure of directionally solidified 1:2:3-2:1:1 composites has been examined using TEM. We have observed polygonization in samples with 30 vol % 2:1:1. These samples did not contain cracks observable with the optical microscope. Polygonalization constitutes a generation mechanism of low angle grain boundaries which is controlled by interfacial energy considerations rather than solidification instabilities as suggested earlier for other melt-processed samples. Many dislocations are observed to originate from the low angle grain boundaries. Thus, polygonization can be regarded also as a dislocation generation mechanism. Typical densities are $\sim 10^9$ dislocations/cm^2, one order of magnitude lower than that reported for other melt-processed samples. This density may however increase locally around 2:1:1 precipitates, especially when the density of precipitates is high.

Stacking faults are inhomogeneously distributed within the superconductive matrix. Moreover, their distribution is consistent with two generation mechanisms which would take place during and after the solidification process, respectively. The first one results from the ability of directionally solidifying 1:2:3 to incorporate Cu in excess from the Cu-rich melt. Such stacking faults are inhomogeneously distributed within the matrix, with typical densities of $\sim 10^{14}$ faults/cm^{-3} and lengths $\sim 6\times 10^{-5}$ cm. Their final distribution is probably controlled by the stress state created during solidification and subsequent thermal cycling. The second type appear intimately associated to the 2:1:1/1:2:3 interface along segments which are normal to the matrix *a-b* planes. Their origin was related to the dissolution of 2:1:1 precipitates. However, for the time being it is not possible to conclude that there is a net increase of the density of stacking faults with increasing density of 2:1:1 precipitates.

Samples with 30 vol % 2:1:1 do not contain cracks observable with the optical microscope. However TEM observations show that they contain a high density of small microcracks which are effectively stopped by 2:1:1 precipitates. The average microcracks contain typically a highly defective layer as well as Cu-rich material inside them. Both features are probably related to decomposition effects of the 1:2:3 phase.

Examination of the 2:1:1/1:2:3 interfaces indicated that they are undisturbed on the atomic scale along segments far from stacking-fault agglomerations. Interpretation of SAD patterns measured across several interfaces led us to conclude that there is a tendency of 2:1:1 to optimize their interface orientation with the 1:2:3 matrix. Generally, a correspondence between high index directions and planes of precipitate and matrix was found. However, no overall texture of the 2:1:1 phase embedded in the 1:2:3 matrix could be detected from the ESR spectra recorded at different sample orientations with the external field.

The observed sharp 2:1:1/1:2:3 interfaces will certainly have a very relevant effect on the macroscopic pinning force of the 1:2:3-2:1:1 composites but their dominant role will depend on field orientation and field strength because the other pinning mechanisms are essentially anisotropic. A strong magnetic-field dependence of the pinning force associated with 2:1:1/1:2:3 interfaces and the still relatively high dilution of the 2:1:1 precipitates are the key factors in the fact that at high vortex densities, i.e., at high magnetic fields, critical currents are not actually limited by this pinning mechanism. Other pinning centers should be considered as well in this case and then it is a complex matter to evaluate the relative contribution of the different defects to the observed critical currents.

ACKNOWLEDGMENTS

This work has been supported by: MIDAS program (93-2331), CICYT (MAT91-0742), and CEE-SCIENCE [SCI-0389-M(A)]. F.S. acknowledges the Generalitat de Catalunya a CIRIT for support. We are very grateful to Dr. B. Martínez for sharing his unpublished data with us, and Dr. J. Fontcuberta for fruitful suggestions and comments. Finally, we also thank Dr. José Vidal for performing the ESR measurements.

[1]S. Jin, T. H. Tiefel, R. C. Sherwood, R. V. van Dover, M. E. Davis, G. W. Kammlott, and R. A. Fastnacht, Phys. Rev. B **37**, 7850 (1989); S. Jin, T. H. Tiefel, R. C. Sherwood, M. E. Davis, R. B. van Dover, G. W. Kammlott, R. A. Fastnacht, and H. D. Keith, Appl. Phys. Lett. **52**, 2074 (1988).

[2]K. Salama, V. Selvamanickam, L. Gao, and K. Sun, Appl. Phys. Lett. **54**, 2353 (1989).

[3]M. Murakami, Mod. Phys. Lett. **4**, 163 (1990).

[4]M. Murakami, M. Morita, and N. Koyama, Jpn. Appl. Phys. **28**, L1125 (1989).

[5]P. J. McGuinn, W. Chen, N. Zhu, M. Lanagan, and U. Balanchandran, Appl. Phys. Lett. **57**, 1455 (1990).

[6]V. Selvamanickam, C. Partsinevelos, A. V. McGuire, and K. Salama, Appl. Phys. Lett. **60**, 3313 (1992).

[7]T. Izumi and Y. Shiohara, J. Mater. Res. **7**, 16 (1992).

[8]S. Piñol, V. Gomis, B. Martínez, A. Labarta, J. Fontcuberta, and X. Obradors, J. Alloys Compounds **195**, 11 (1993).

[9]M. Brand, C. Gross, S. Elschner, S. Gauss, and W. Assmus (un-

published); S. Elschner, W. Becker, H. Bestgen, and M. Brand, Physica C **202**, 401 (1992).
[10]H. Wang, H. Herman, H. J. Wiesman, Y. Zhu, Y. Xu, R. L. Sabatini, and M. Suenaga, J. Appl. Phys. **57**, 2495 (1990).
[11]N. Okzan, B. A. Glowacki, E. A. Robinson, and P. A. Freeman, J. Mater. Res. **6**, 1829 (1991).
[12]J. Chunlin, F. Zhanguo, Z. Guofan, Z. Guiyi, B. Weimin, Z. Zhongxian, and G. Shuquan, Supercond. Sci. Technol. **4**, 49 (1991).
[13]A. Goyal, P. D. Funkenbusch, D. M. Kroeger, and S. J. Burns, Physica C **182**, 203 (1991).
[14]Y.-L. Wang, H. J. Wiesmann, C. F. Liu, Y. Zhu, R. L. Sabatini, and M. Suenaga, J. Appl. Phys. **74**, 4052 (1993).
[15]J. Mannhart and C. C. Tsuei, Z. Phys. B **77**, 53 (1989).
[16]K. B. Alexander, A. Goyal, D. M. Kroeger, V. Selvamanickam, and K. Salama, Phys. Rev. B **45**, 5622 (1992).
[17]V. Selvamanickam and K. Salama, Appl. Phys. Lett. **57**, 1575 (1990).
[18]A. Goyal, K. B. Alexander, D. M. Kroeger, P. D. Funkenbusch, and S. J. Burns, Physica C **210**, 197 (1993).
[19]G. J. Schmitz, J. Laakmann, Ch. Wolters, S. Rex, W. Gawalek, T. Habisreuther, G. Bruchlos, and P. Görnert, J. Mater. Res. **8**, 2774 (1993).
[20]F. Sandiumenge, S. Piñol, and X. Obradors (unpublished).
[21]H. Fujimoto, T. Taguchi, M. Murakami, N. Nakamura, and N. Koshizuka, Cryogenics **32**, 954 (1992).
[22]W. K. Kwok, U. Welp, G. W. Crabtree, K. G. Vandervoort, R. Hulscher, and J. Z. Liu, Phys. Rev. Lett. **64**, 966 (1990).
[23]V. M. Pan, V. L. Strechnikov, V. F. Solovjov, V. F. Taborov, H. W. Zandbergen, and J. G. Won, Supercond. Sci. Technol. **5**, 707 (1992).
[24]V. Selvamanickam, M. Mironova, S. Son, and K. Salama, Physica C **208**, 238 (1993).
[25]S. Jin, T. H. Tiefel, S. Nakahara, J. E. Graebner, H. M. O'Bryan, R. A. Fastnacht, and G. W. Kammlott, Appl. Phys. Lett. **56**, 1287 (1990).
[26]Z. L. Wang, A. Goyal, and D. M. Kroeger, Phys. Rev. B **47** 5373 (1993).
[27]B. Martínez, V. Gomis, S. Piñol, I. Catalán, J. Fontcuberta, and X. Obradors, Appl. Phys. Lett. **63**, 3081 (1993).
[28]M. Murakami, S. Gotoh, N. Koshizuka, S. Tanaka, T. Matsushita, S. Kanube, and K. Kitazawa, Cryogenics **30**, 390 (1990); M. Murakami, S. Gotoh, H. Fujimoto, K. Yamaguchi, N. Koshizuka, and S. Tanaka, Supercond. Sci. Technol. **4**, S43 (1991).
[29]S. Jin, T. H. Tiefel, and G. W. Kammlot, Appl. Phys. Lett. **59**, 540 (1991).
[30]P. McGuinn, N. Zhu, Q. Chen, S. Sengupta, and T. Li, Physica C **176**, 203 (1991).
[31]D. Shi, H. Krishnan, J. M. Hong, D. Miller, P. J. McGuinn, W. H. Chen, Ming Xu, J. G. Chen, M. M. Fang, U. Welp, M. T. Lanagan, K. C. Goretta, J. T. Dusek, J. J. Picciolo, and U. Balachandran, J. Appl. Phys. **68**, 228 (1990).
[32]M. Murakami, H. Fujimoto, S. Gotoh, K. Yamaguchi, N. Koshizuka, and S. Tanaka, Physica C **185-189**, 321 (1991); M. Murakami, T. Oyama, H. Fujimoto, S. Gotoh, K. Yamaguchi, Y. Shiohara, N. Koshizuka, and S. Tanaka, IEEE Trans. Magn. **MAG-27**, 1479 (1991).
[33]V. Gomis, S. Piñol, B. Martínez, J. Fontcuberta, and X. Obradors (unpublished); B. Martínez *et al.* (unpublished).
[34]K. Yamaguchi, M. Murakami, H. Fujimoto, S. Gotoh, T. Oyama, Y. Shiohara, N. Koshizuka, and S. Tanaka, J. Mater. Res. **6**, 1404 (1991).
[35]K. Yamaguchi, M. Murakami, H. Fujimoto, N. Koshizuka, and S. Tanaka, Physica C **185-189**, 2497 (1991).
[36]A. Goyal, W. C. Oliver, P. D. Funkenbusch, D. M. Kroeger, and S. J. Burns, Physica C **183**, 221 (1991), and references therein.
[37]M. Mironova, D. F. Lee, and K. Salama, Physica C **211**, 188 (1993).
[38]S. Gauss, S. Elschner, and H. Bestgen, Cryogenics **32**, 964 (1992).
[39]M. Ullrich, D. Müller, K. Heinemann, L. Niel, and H. C. Freyhardt, Appl. Phys. Lett. **63**, 406 (1993); M. Ullrich, D. Müller, W. Mexner, M. Steins, K. Heinemanm, and H. C. Freyhardt, Phys. Rev. B **48**, 7513 (1993).
[40]R. W. Cahn, in *Physical Metallurgy,* edited by R. W. Cahn and P. Haasen (Elsevier Science BV, New York, 1983), Chap. 25, p. 1596.
[41]D. R. Uhlmann, B. Chalmers, and K. A. Jackson, J. Appl. Phys. **35**, 2986 (1964).
[42]K. Salama, V. Selvamanickam, and D. F. Lee, in *Processing and Properties of High-T_c Superconductors,* edited by Sungho Jin (World Scientific, Singapore, 1993), Vol. 1, p. 155.
[43]Y. Zhu, H. Zhang, H. Wang, and M. Suenaga, J. Mater. Res. **6**, 2507 (1991).
[44]J. Rabier and M. F. Denanot, Philos, Mag. A **65**, 427 (1992).
[45]H. Gu, C. Colliex, S. Senoussi, C. Aguillon-Levillain, and P. Manuel, Philos. Mag. A **68**, 19 (1993).
[46]J. Tafto, M. Suenaga, and R. L. Sabatini, Appl. Phys. Lett. **52**, 667 (1988).
[47]H. W. Zandbergen, R. Gronsky, and G. Thomas, Phys. Status Solidi A **105**, 207 (1988).
[48]A. F. Marshall, K. Char, R. W. Barton, A. Kapitulnik, and S. S. Laderman, J. Mater. Res. **5**, 2049 (1990).
[49]R. Ramesh, D. M. Hwang, T. S. Ravi, A. Inam, X. D. Wu, and T. Venkatesan, Physica C **171**, 14 (1990).
[50]J. Zheng, Q. Li, D. Feng, S. Ding, S. Yu, G. Shen, F. Liu, L. Zhou, and H. Mou, J. Appl. Phys. **72**, 4634 (1992).
[51]W. Geya, S. Tiansheng, F. Yaoxian, C. Chuanbing, and Y. Hongchuan, Supercond. Sci. Technol. **6**, 657 (1993).
[52]B. Domenges, M. Hervieu, C. Michel, and B. Raveau, Europhys. Lett. **4**, 211 (1987).
[53]R. K. Williams, K. B. Alexander, J. Brynestad, T. J. Henson, D. M. Kroeger, T. B. Lindemer, G. C. Marsh, J. O. Scarbrough, and E. D. Specht, J. Appl. Phys. **70**, 906 (1991).
[54]J. Karpinsky, S. Rusiecki, E. Kaldis, B. Bucher, and E. Jilek, Physica C **160**, 449 (1989).
[55]N. Chen, S. J. Rothman, J. L. Routbort, and K. C. Goretta, J. Mater. Res. **7**, 2308 (1992).
[56]H. Fujimoto, M. Murakami, and N. Koshizuka, Physica C **203**, 103 (1992).
[57]Diffract 1.5a, Virtual Laboratories, 37 Highland Court, Ukiah, CA 95482.
[58]David C. Johnston, J. Magn. Magn. Mater. **100**, 218 (1991).
[59]R. J. Barham and D. C. Doetschman, J. Mater. Res. **7**, 565 (1992).
[60]N. Pellerin, M. Gervais, and P. Odier, J. Mater. Res. **7**, 558 (1992).
[61]N. Pellerin, Ph.D. these, Universite d'Orleans, 1992.
[62]P. Chaudhari, J. Mannhart, D. Dimos, C. C. Tsuei, J. Chi, M. M. Oprysko, and M. Scheuermann, Phys. Rev. Lett. **60**, 1653 (1988); D. Dimos, P. Chaudhari, J. Mannhart, and F. L. Legoues, *ibid.* **61**, 219 (1988); D. Dimos, P. Chaudhari, and J. Mannhart, Phys. Rev. B **41**, 4038 (1990).

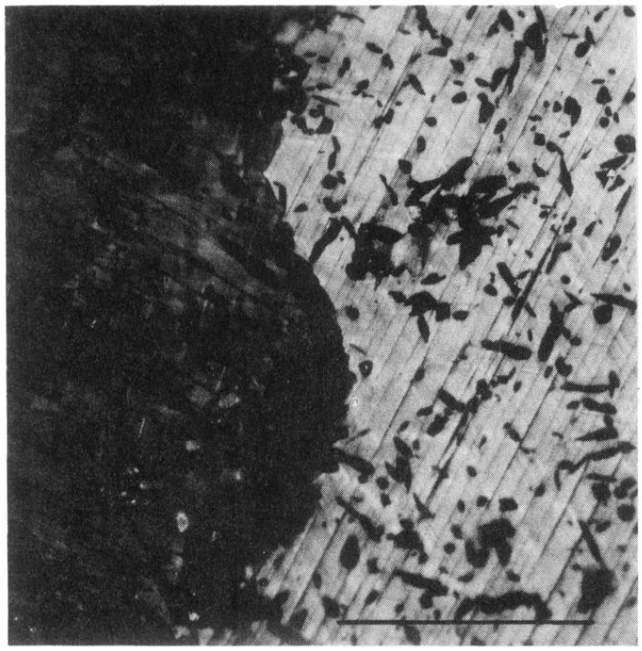

FIG. 1. Grain boundary corresponding to two domains misoriented by 90° in a sample with ~15 vol % 2:1:1. The growth axis is vertical. Scale bar represents 50 μm.

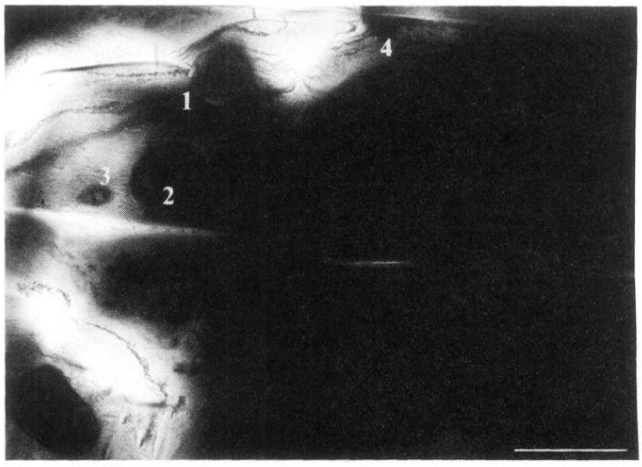

FIG. 10. TEM image of a region containing several precipitates with different sizes. The relative orientations of precipitates 1–4 were determined. The scale bar corresponds to 1 μm.

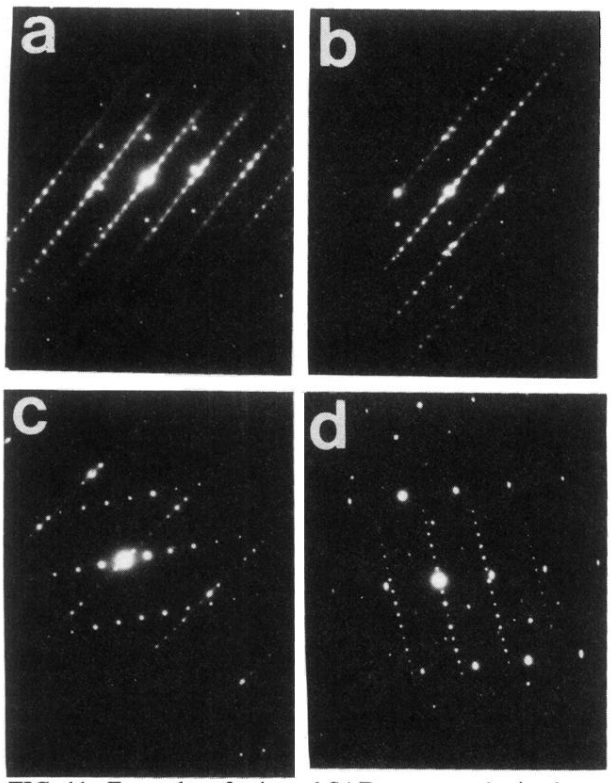

FIG. 11. Examples of oriented SAD patterns obtained across different 2:1:1/1:2:3 interfaces. The four patterns manifest parallelism between particular directions of precipitate and matrix.

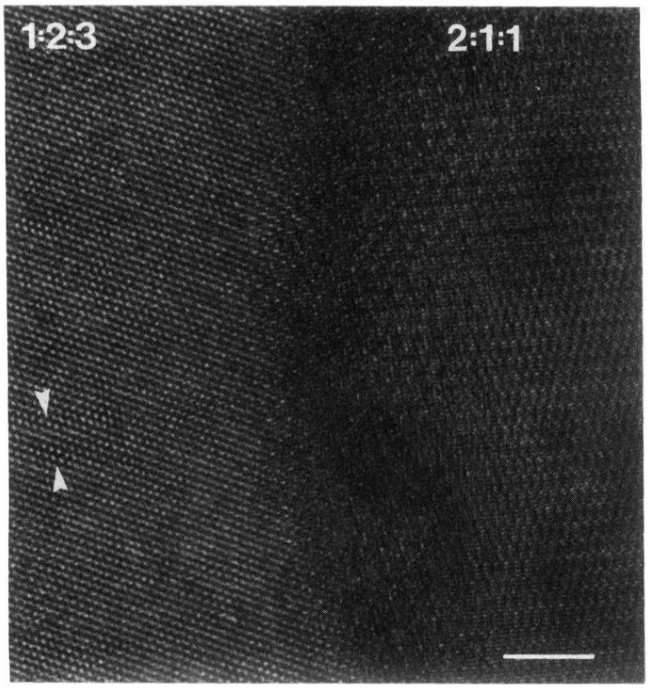

FIG. 12. HRTEM image of a 2:1:1/1:2:3 interface. The zone axes are [331] and [−211] for 1:2:3 and 2:1:1, respectively. Arrowheads indicate small dislocations. Scale bar corresponds to 4 nm.

FIG. 2. Polygonization effect in a single domain with ~30 vol% 2:1:1. The grain boundary indicated by A is sharp, in contrast to that at the left-hand side of letter B. Scale bar 50 μm.

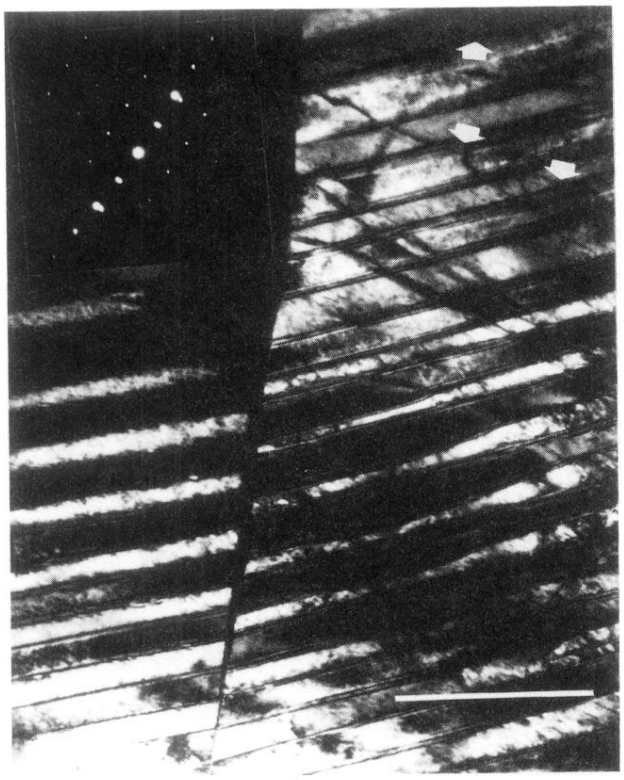

FIG. 3. TEM image viewed along the [001] direction showing a nearly pure 5°−[001] twist boundary. Note that several dislocations originate from the grain boundary. The inset presents the SAD pattern obtained across the boundary. Scale bar represents 0.5 μm.

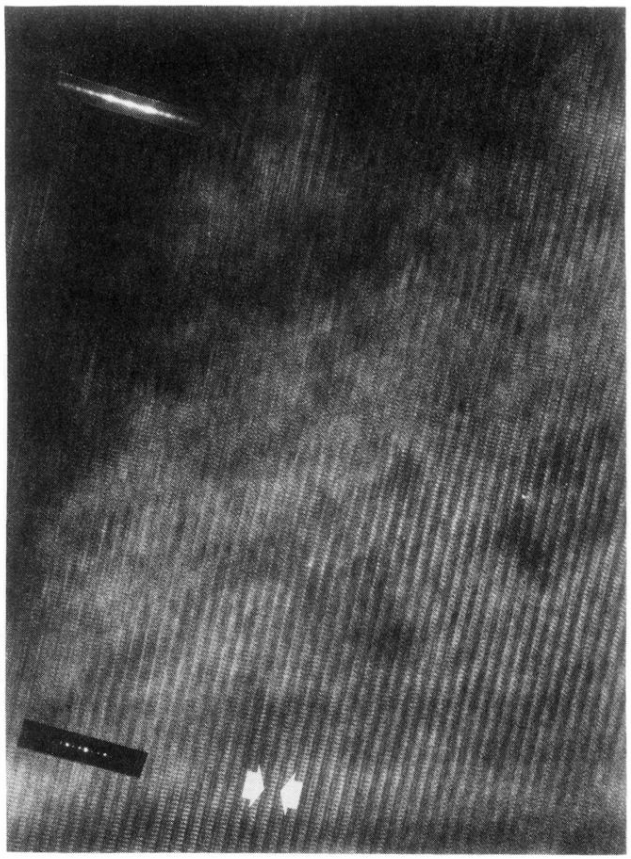

FIG. 4. HRTEM image viewed along the [100] direction showing a transition from a well-ordered zone (left-hand side) to a highly defective one (right-hand side of the micrograph) in the 1:2:3 matrix along its associated SAD patterns. Distance between arrow tips equals 1.17 nm.

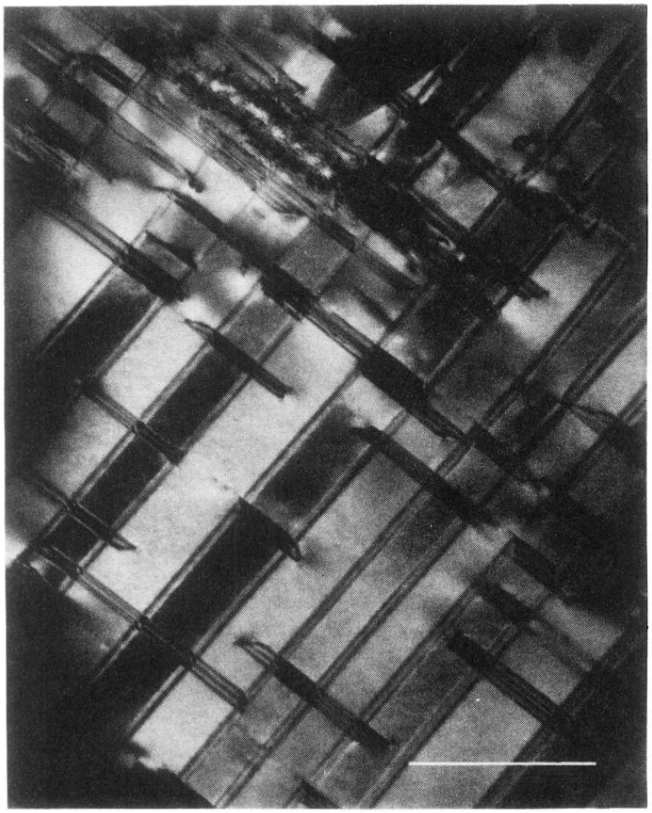

FIG. 5. TEM image viewed along the [3 −6 1] direction of a 1:2:3 matrix region in a sample with 15 vol % 2:1:1 displaying twin boundaries and stacking faults. Scale bar corresponds to 0.25 μm.

FIG. 6. Lattice fringe image corresponding to the [100] zone axis of a region close to that shown in Fig. 5. Note the high density of stacking faults. Scale bar corresponds to 25 nm.

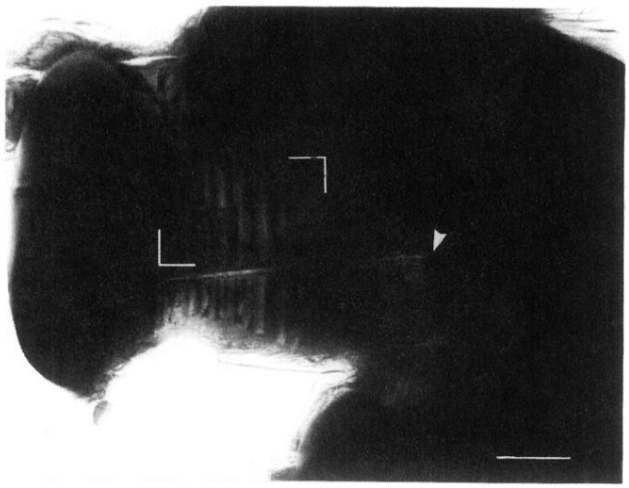

FIG. 7. TEM image corresponding to the [100] zone axis of a sample with ~30 vol % 2:1:1. The matrix between precipitates is highly defective. In particular the area enclosed between square marks contains stacking faults and twin boundaries. A microcrack which is stopped *within* a 2:1:1 precipitate is indicated by an arrow head. Scale bar corresponds to 1 μm.

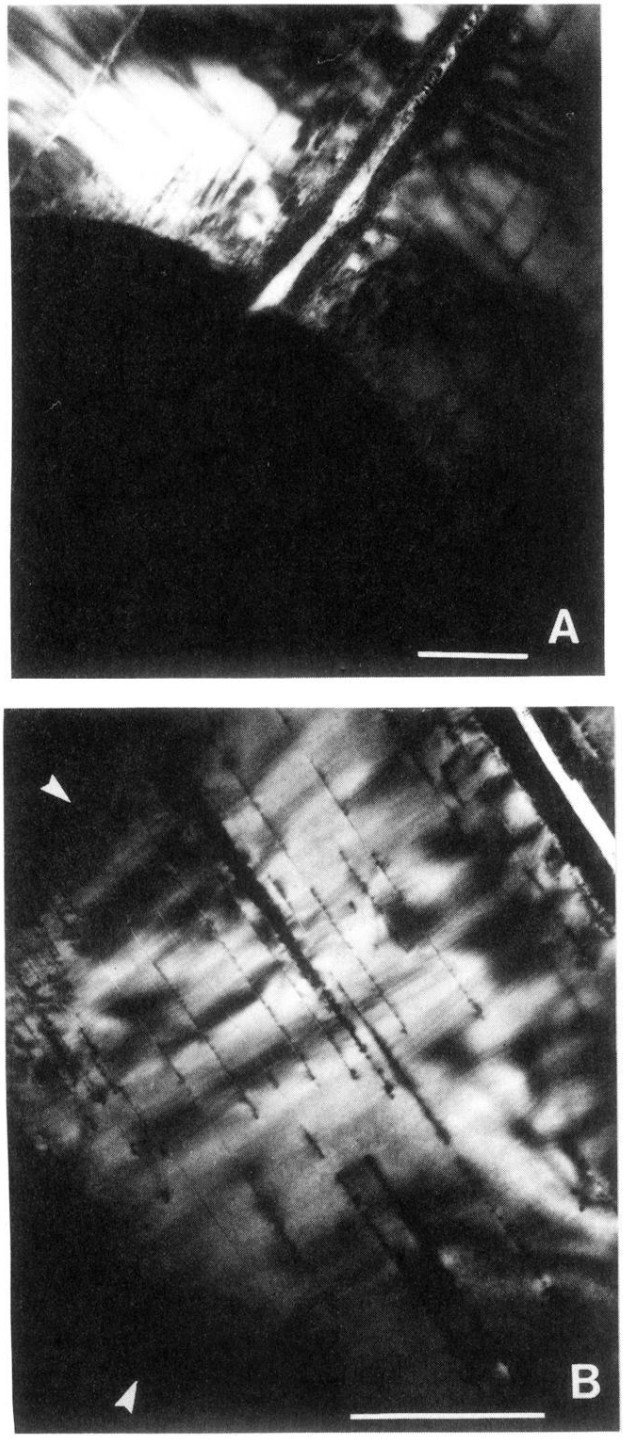

FIG. 8. Stacking faults associated to the interaction of a microcrack and a 2:1:1 precipitate (A), and a 2:1:1/1:2:3 interface nearly perpendicular to the *a-b* planes (B). Both images viewed along [100] direction. Scale bars represent 0.5 μm.

FIG. 9. TEM image of a 2:1:1 precipitate intercepted by a microcrack at places arrowed in the figure. The region between both intercepts shows a complex dislocation network. The arrowhead indicates Y_2O_3 inclusions. The scale bar corresponds to 0.5 μm.